Journal Name

Preprint submitted to Journal of Materials Chemistry A (October 2105)

ROYAL SOCIETY OF CHEMISTRY

ARTICLE

The A-cation Deficient Perovskite Series $La_{2-x}CoTiO_{6-\delta}$ ($0 \le x \le 0.20$): New Potential Cathodes for Solid Oxide Fuel Cells

Received 00th January 20xx,
Accepted 00th January 20xx

DOI: 10.1039/x0xx00000x

www.rsc.org/

Alejandro Gómez-Pérez[*,a], M.Teresa Azcondo[a], Mercedes Yuste[a], Juan Carlos Pérez-Flores[a], Nikolaos Bonanos[b], Florence Porcher[c], Alvaro Muñoz-Noval[d], Markus Hoelzel[e], Flaviano García-Alvarado[*,a] and Ulises Amador[a].

$La_{2-x}CoTiO_{6-\delta}$ are presented as promising new cathode materials for solid oxide fuel cells. The B-site ordering characteristic of double perovskites is present in the whole series. Additionally, increasing amounts of La-vacancies gives rise to ordering of alternating La-rich and □-rich (□ = vacancy) layers perpendicular to the c-axis. The introduction of La vacancies produces both oxidation of Co^{2+} to Co^{3+} and oxygen vacancies inducing a change of both electrical and electrochemical properties. The best electrochemical performances are obtained for low x due to a compromise between sufficiently high amount of defects to provide electronic and ionic conductivities, but not so high to induce defect clustering. The material with x= 0.05 exhibits the best performances of the series. Symmetrical cells made of composites of this material and $Ce_{0.9}Gd_{0.1}O_{2-\delta}$ deposited on pellets of this electrolyte show a polarization resistance of 0.39 Ωcm^2 at 1073 K

Introduction

Perovskite oxides, which are a highly versatile and easily controllable family of compounds, have triggered intensive research due to their potential application in several types of solid-state electrochemical devices for electrical power generation.[1-4] Regarding applications as cathode materials, the most interesting aspect, from both the structural and chemical points of view, is the large variety of metal ions the structure can accept. Those with variable oxidation states may change the material's electronic properties under different atmospheres or upon aliovalent substitution. Moreover, the anionic sub-lattice tolerates a considerable amount of vacancies. It is thus common that properly tuned perovskite exhibit both mixed ionic-electronic conductivity (MIEC) which combined with high catalytic activity make these compounds of considerable interest as electrode materials [5-7] for solid oxide fuel cells (SOFCs). To date, perovskite oxides have been extensively used in the development of new electrode materials in both high- and intermediate-temperature devices (IT-SOFCs). In any of them, oxygen vacancies in the MIEC perovskites are needed to enable oxygen ion transport through the cathode.

Improvement of the electronic conductivity can be achieved by inducing mixed oxidation states in B-site ions, whereas creation of oxygen vacancies is not so directly obtained as it depends also on the predominant charge compensation mechanism in the cationic sites.

Cobalt-based perosvkites have been intensively investigated due to their high activity for oxygen reduction reaction.[8-10] However, problems may arise due to structural stability, chemical and thermal compatibility.[11]

The most investigated cathode material, $La_{1-x}Sr_xMnO_3$ (LSM), was attained by substitution of La^{3+} by Sr^{2+}. Aliovalent substitution improves electronic conductivity (due to small polaron hopping related to the manganese mixed oxidation

[a.] Universidad CEU San Pablo, Facultad de Farmacia, Departamento de Química y Bioquímica, Urb. Montepríncipe, Boadilla del Monte, E-28668, Madrid, Spain.
[b.] Department of Energy Conversion and Storage Technical University of Denmark, Risø Campus, DK-4000 Roskilde, Denmark.
[c.] Laboratoire Léon Brillouin, Centre d'Etudes de Saclay, 91191 Gif-sur-Yvette Cedex, France..
[d.] SpLine Spanish CRG Beamline, ESRF, 6 Rue J. Horowitz, Grenoble, Isere/Rhone-Alpes, 38042, France.
[e.] Forschungsneutronenquelle Heinz Maier-Leibnitz(FRM II), Technische Universität München, Lichtenbergstrasse 1, D-85747 Garching, Germany.

Electronic Supplementary Information (ESI) available: Figure SI 1: XRD patterns at RT for $La_{2-x}CoTiO_{6-\delta}$ ($0.05 \le x \le 0.25$) series. Figure SI 2: Back-scattered electron scanning image of a pellet of $La_{1.75}CoTiO_6$. Figure SI 3: XRD pattern at RT of a sample of composition $La_{1.80}CoTiO_{6-\delta}$ after electrical measurements under a reducing atmosphere. Figure SI 4: NPD patterns at RT for $La_{2-x}CoTiO_{6-\delta}$ ($0.05 \le x \le 0.20$) series. Figure SI 5: Thermal evolution of NPD super-structure peaks of $La_{1.85}CoTiO_{6-\delta}$. Figure SI 6: NPD patterns at 1073 K for $La_{2-x}CoTiO_{6-\delta}$ (x= 0.05 and 0.15). Figure SI 7: Backscattered electron micrographs and elemental distribution in bar of $La_{1.80}CoTiO_{6-\delta}$ after electrical measurements under reducing conditions. Figure SI 8: Variation of the resistance with time upon a change of pO_2 from 0.21 atm to 1.00 atm for a sample of composition $La_{1.80}CoTiO_{6-\delta}$. Figure SI 9: XRD-pattern of $La_{1.90}CoTiO_{6-\delta}$:YSZ (1:1 w:w) composite after fired at high temperature 8h. Table SI 1: Structural parameters for $La_{2-x}CoTiO_{6-\delta}$ obtained from XRD and NPD data. Table SI 2: Selected structural information for $La_{2-x}CoTiO_{6-\delta}$. Table SI 3: Structural parameters for $La_{2-x}CoTiO_{6-\delta}$ (x=0.05 and 0.15) at 1073 K obtained from SXRD and NPD data.
]. See DOI: 10.1039/x0xx00000x

state, Mn^{3+}/Mn^{+4}) with respect to the parent $LaMnO_3$. Since then, Sr has been used as a common substituent of similar size to La in LaMO3 perovskites in search of both anode and cathode materials.[12-22]

Interestingly, in the case of $La_{2-x}Sr_xCoTiO_{6-\delta}$ series, La/Sr replacement produces a significant increase of electronic conductivity (from 3.6 10^{-2} Scm^{-1} to 1.4 Scm^{-1} for the parent compound and x = 0.4, respectively) inasmuch as the sole charge compensation mechanism is the oxidation of Co^{2+} to Co^{3+}. The lack of oxygen vacancies seemed to limit its electrochemical performances ($La_{1.60}Sr_{0.40}CoTiO_{6-\delta}$ based electrodes exhibit polarization resistances of 0.8 Ωcm^2 at 1073 K in oxygen).[22]

On the one hand, the same aliovalent replacement (La^{3+} by Sr^{2+}) in $La_{2-x}Sr_xNiTiO_{6-\delta}$ produces a large amount of oxygen vacancies and little oxidation of Ni^{2+} and again a very significant increase of electrical conductivity. However, electrochemical performances are good enough[21]. Interestingly, La deficiency ($La_{2-x}NiTiO_{6-\delta}$) instead of aliovalent substitution yielded a more promising cathode material (R_p ~0.5 $\Omega\,cm^2$ at 1073 K for the x=0.2 member).[23]

On the other hand, it is very well known that the presence of alkaline-earth metals, as Sr, increases the basicity of the perovskite and consequently the reactivity towards CO_2.[24] A low tolerance to CO_2(g) impurities is an important drawback for IT-cells,[25-30] so that alkaline-earth metal-free perovskites can alleviate the problem. Therefore, we considered that a best approach to obtain promising cathode material in the $LaCoTiO_6$ system is the introduction of La vacancies instead of replacement by Sr.

Many other aspects may hinder the use of some perovskites as the cathode of SOFC. Among others, one could mention the mechanical strength and chemical stability under oxidizing atmospheres, as well as side reactions with other cell components at high temperature. [31, 32] In this connection, it is very well known that LSM reacts with yttria-stabilized zirconia (YSZ) above 1200°C. Therefore, co-sintering of the electrolyte and cathode has to be performed below that temperature[33-35]. Chemical instability can be also cured in some cases by the creation of vacancies in the A-site [2, 29, 36-38]. Indeed, some A-deficient perovskites exhibit high thermal stability and chemical compatibility while maintaining good electrochemical characteristics.[39]

Herein, we present the $La_{2-x}CoTiO_{6-\delta}$ ($0.05 \le x \le 0.20$) series. A detailed chemical and structural characterization, using both conventional and synchrotron X-ray radiation, and neutron powder diffraction, has been carried out to fully determine its defect chemistry. Besides, the electrical and electrochemical properties have been analyzed on the basis of the defect chemistry, and compared to those of the previously reported $La_{2-x}Sr_xCoTiO_{6-\delta}$ ($0 \le x \le 1.0$) series. Important differences have been found regarding the defect chemistry that affects the electrochemical performances. In particular the x=0.05 series member is presented as a promising cathode material for SOFC.

Experimental

Samples preparation

The synthesis of the $La_{2-x}CoTiO_{6-\delta}$ materials (with x = 0.00, 0.05, 0.10, 0.15, 0.20 and 0.25) was performed using a modified Pechini method. Batches of ca. 10 grams were prepared by dissolving the stoichiometric amounts of $Co(CH_3COO)_2.4H_2O$ (Aldrich, 99,99%), La_2O_3 (Aldrich, 99,9%) in ca. 90 ml of diluted hot nitric acid (4:1 water/nitric acid ratio) under continuous stirring. Afterwards, citric acid was added in a citric-to-metal molar ratio of 3:1 with constant heating and stirring. The stoichiometric amount of insoluble TiO_2 (anatase, Aldrich 99.9%) was then added to obtain a homogeneous suspension. Once the volume was reduced by half, ca. 5 ml of diethylene glycol was added as polymerization agent. The resulting resin was then burned in a sand bath at 250º C for a few hours. The ashes were collected and milled in an agate mortar and then fired at 1073 K for 8 hours to remove all organic matter. The resulting black powders was again milled and pressed into pellets and treated at 1773 K for 60h with a heating/cooling rate of 2 K min^{-1}.

Characterization techniques

The sample purity was determined by powder X-ray diffraction (XRD) on a Bruker D8 high-resolution diffractometer equipped with a rapid LynxEye™ detector, using monochromatic $CuK_{\alpha 1}$ (λ = 1.5406 Å) radiation obtained with a germanium primary monochromator. The angular range, step size and counting time were selected such that the data could also be used for the structure refinement.

The chemical composition of the samples was determined by electron dispersive spectroscopy (EDS) using an EDAX detector on a FEI XL30 scanning electron microscope (SEM) by analyzing about 20 grains of every sample.

Neutron powder diffraction (NPD) experiments were carried out at room temperature in the high-resolution 3T2 powder diffractometer at Laboratoire Leon-Brillouin (Saclay, France). A monochromatic beam of wavelength 1.22525 Å was selected with a Ge (335) monochromator in order to access high Q, the corresponding instrumental resolution being within the range $2.2\ 10^{-3} \le (\Delta Q/Q) \le 0.0092$. Neutron thermo-diffraction from room temperature to 1073 K was performed on the high-resolution powder diffractometer SPODI[40] (Forschungsneutronenquelle Heinz-Maier Leibnitz (FRM II) in Garching, Munich, Germany). A wavelength of λ = 1.5484 Å was selected using a Ge(551) monochromator, the corresponding resolution in this Q-range is 2.2 10-3 ≤ ($\Delta Q/Q$) ≤ 0.0092. Synchrotron radiation high resolution powder X-ray diffraction (SXRD) patterns were collected on the SpLine the Spanish CRG beamline BM25A at the European Synchrotron Radiation Facility (ESRF), Grenoble (France).[41] The sample was finely ground and loaded into a 0.4 mm diameter capillary mounted in a spinning goniometer. Data were collected in a continuous 2θ-scan mode from 7 to 48 with a step size of 0.01 degree, using an incident wavelength of 0.62100(6) Å (calibrated with NIST SRM 640c silicon powder; a=5.431195(9)Å), National Institute of Standards and

Technology); the instrumental resolution in the measured range Q-range is 2.2 10-3 ≤ (ΔQ/Q) ≤ 0.0092. Patterns were collected at different temperatures from ambient to 1073 K; the capillary is heated up by a continuous high-flux stream of hot air and the temperature is monitored on the capillary containing the sample.

Structural refinements were carried out by the Rietveld method using the FullProf program[42] by simultaneous fitting of XRD and NPD data. The neutron scattering amplitudes used in the refinement were 0.824, 0.249, -0.344 and 0.581 (10^{-12}cm) for La, Co, Ti and O, respectively; isotropic thermal factors (ITF) were used for all atoms.

The cobalt oxidation state and oxygen content (assuming charge neutrality) of samples were determined by titration using potassium dichromate, as described in ref.[43]. Independent determinations were performed by thermogravimetric analyses using a D200 Cahn Balance. Typically, ca. 70 mg of the sample were weighed to a precision of ±0.0005 mg at a total reduced pressure of 400 mbar containing 60% He and 40% H_2. The sample was then heated to 1173 K at a rate of 5 K min^{-1}.

Total electrical conductivity was measured by the four-probe DC method on bars of ca. 2 x 4 x 14 mm^3 dimensions and relative densifications of 90% of the crystallographic density. The bars were prepared by ground milling of the powders, isostatic pressing at 200 MPa and sintering at 1773 K for 6 hours. Platinum electrodes were attached to each extreme of the bar with a Pt-paste (Metalor); to eliminate the organic matter from the paste and ensure good electrical contact an annealing treatment at 1373 K for 2 hours was applied. DC-electrical measurements were performed using a Keithley 580 Micro-Ohmmeter controlled using in-house software. Data were collected in the temperature range 673-1173 K at 25 K intervals. Isothermal experiments were also carried out at 1073 K varying the atmosphere under a continuous flow of 100 ml min^{-1} obtained by blending air, O2, H_2(9%)/N_2(91%) or pure H_2 with N_2. Samples were held for 4 h in the corresponding atmospheres at each temperature, except when changing from 100% N2 to N2/H2 mixture when they were held for 12 h, to ensure full equilibration.

The chemical compatibility of the electrode materials based on $La_{2-x}CoTiO_{6-\delta}$ series with the commercial electrolytes YSZ8 (YSZ (8%), Tosoh) and CGO10 (CGO, Fuel Cell Materials) was evaluated by mixing the material with either YSZ or CGO in a 1:1 w:w ratio. Mixtures were pelletized and heated at 1273 K for 12 h or 1073 K for 3 days under air; phase analysis was then performed by XRD.

Slurries for symmetrical-cell measurements were prepared by mixing the as-prepared materials with YSZ or CGO powders in 1:1 w:w ratio with Decoflux (WB41, Zschimmer and Schwarz) as a binder. The electrodes were prepared by coating both sides of dense YSZ and CGO disks (thickness ≈ 1 mm) with the slurries using active areas of 6 mm diameter. The resulting assemblies were fired at 1273K for 8 hours, and then a Pt-based paste was deposited onto the electrodes with a platinum wire attached and fired again for 2 hours at 1173 K.

Polarization measurements were performed with a two-electrode arrangement, as previously reported.[44] Impedance-spectroscopy measurements of cells were carried out using a Solartron 1260 frequency response analyzer (FRA) by applying a 100 mV AC signal in the 10^6-10^{-1} Hz range over the temperature range of 573-1173 K in air. Electrode microstructure was investigated by SEM before and after polarization measurements.

Results and Discussion

Compositional range and chemical stability

Single-phase samples at the resolution of XRD were obtained for compositions 0.05 ≤ x ≤ 0.25 of the $La_{2-x}CoTiO_{6-\delta}$ series (Figure SI 1 of electronic supporting information, ESI). This range seems to be slightly greater than that reported in a previous paper [23] for the analogous Ni-containing series in which the limit for La vacancies was found at x ≈ 0.20. However, the SEM and EDS studies of samples with the highest level of A-site vacancies, i.e. x = 0.25, revealed the presence of some segregated lanthanum-poor and cobalt-rich phase (Fig. SI 2) suggesting off-stoichiometry in this sample.

EDS analyses were performed using a scanning electron microscope, confirming the actual compositions of samples with x≤ 0.20, listed in Table 1, to be the nominal ones. The Ti- and Co-contents are similar for all members of the $La_{2-x}CoTiO_{6-\delta}$ (0 ≤ x ≤ 0.20) series, in contrast to the case of the Ni-containing analogous materials in which the Ti/Ni ratio is always greater than the nominal one (1:1). Table 1 also shows the NPD refined composition which confirms that the metal contents are close to the nominal ones and that no segregation of secondary phases has occurred.

In our previous study of $La_{2-x}NiTiO_{6-\delta}$ perovskites[23] we concluded that the structure cannot tolerate a large amount of either A-site or anion vacancies, the limit of the series being x ≈ 0.20; this seems to be now confirmed for the Co-containing analogues. However, an important difference between the two series of A-deficient perovskites is observed: since Ni^{2+} is hardly oxidized, excess Ti^{4+} replaces part of the Ni^{2+} to compensate partially the positive charge loss due to A-site vacancies. By contrast, as Co^{3+} is common in oxides[45] Ti-overstoichiometry is not observed in the $La_{2-x}CoTiO_{6-\delta}$ series.

The $La_{2-x}CoTiO_{6-\delta}$ oxides are stable in air up to the melting point, slightly higher than the synthesis temperature used, above which they melt incongruently with segregation of several phases. They are also stable under reducing atmospheres. As an example, Fig. SI 3 shows the XRD patterns corresponding to a sample with composition $La_{1.80}CoTiO_{6-\delta}$ after one-week treatment at $pO_2 \approx 10^{-25}$ atm at 1073 K: no decomposition is observed the only effect being a slight expansion of the unit cell as a result of the reduction of Co^{3+} present in the as-prepared material (see below).

TABLE 1: Metal contents of the $La_{2-x}CoTiO_{6-\delta}$ samples obtained by EDS-SEM and compositions from NPD.

Nominal x	Element content (atom %)			Composition
	La	Co	Ti	
0.05	49.6(6)	24.6(6)	25.8(6)	$La_{1.96(1)}Co_{1.00(1)}Ti_{1.00(1)}O_{5.98(1)}$
0.10	48.9(6)	24.8(6)	26.3(6)	$La_{1.92(1)}Co_{1.00(1)}Ti_{1.00(1)}O_{5.91(1)}$
0.15	48.0(7)	26.5(6)	25.5(6)	$La_{1.86(1)}Co_{1.00(1)}Ti_{1.00(1)}O_{5.84(1)}$
0.20	47.8(6)	26.1(6)	26.1(6)	$La_{1.82(1)}Co_{1.00(1)}Ti_{1.00(1)}O_{5.78(1)}$

Room temperature structure

In a previous paper[23] combining different diffraction techniques such as SAED and HRTEM, XRD and NPD we determined the structures of the $La_{2-x}NiTiO_{6-\delta}$ materials analogous to those reported in this work. As discussed below, we used those structural models as starting points for refining XRD and NPD of the title compounds. Beside, in a recent paper[46] we determined the structure of La_2CoTiO_6 from NPD and synchrotron X-ray diffraction data, to be monoclinic (S.G. $P2_1/n$ (#14) with a unit cell $\sqrt{2}a_p$ x $\sqrt{2}a_p$ x $2a_p$. The monoclinic angle is very close to 90º, the lowering in symmetry with respect to S.G. Pnma (#62), very common in perovskites, being mainly due to the ordering of Ti and Co in the B' and B'' positions of the structure. In the orthorhombic model, there is only one crystallographic site, 4b (0 0 ½), for B cations, i.e. the symmetry does not allow B-cation ordering. By contrast, in the monoclinic model, the 4b site in Pnma can be split into two independent crystallographic sites, 2d (½ 0 0) and 2c (½ 0 ½), which allows an ordered arrangement of the B cations. Since the neutron scattering amplitudes of Co and Ti are significantly different, the site occupancies can be readily determined; this is not the case for XRD, since the X-ray scattering factors of titanium and cobalt are too similar. In the parent compound La_2CoTiO_6, Co^{2+} and Ti^{4+} are ordered, though some degree of intermixing or anti-site defects (AS) of Co and Ti on the B' and B'' sites, respectively, is present (c.a. ~9%). This is a degree of inversion similar to that observed in the Ni-analogous. In contrast to what is observed for this latter, which is slightly Ni-deficient, in La_2CoTiO_6 the actual Ti/Co ratio proves to be 1:1 within the experimental error.

For the $La_{2-x}CoTiO_{6-\delta}$ ($0.05 \leq x \leq 0.20$) series, no phase segregation is observed by XRD, NPD or SEM, only for x=0.25 a cobalt-rich phase is observed by SEM but not in the XRD pattern (see Fig. SI 1). Therefore we used the nominal compositions, confirmed by EDS and shown in Table 1, as the starting point for fitting the diffraction data. As structural starting models we used those corresponding to the analogous Ni-containing materials.

Table SI 1 of ESI collects the refined structural parameters of the $La_{2-x}CoTiO_{6-\delta}$ series (x=0.05, 0.10 and 0.20) as obtained from XRD and NPD data. Selected structural information is given in Table SI 2. As an example, Fig. 1 shows the graphic result of the fitting of the NPD pattern for $La_{1.80}CoTiO_{6-\delta}$ to the corresponding structural parameters (the patterns corresponding to the rest of the series are given in Fig. SI 4).

Oxides of the $La_{2-x}CoTiO_{6-\delta}$ series display perovskite tolerance factors, t, below unity (Table SI 2) as a result of the mismatch between the A-O and B-O bonds. This leads to tilting of the $B'O_6$ and $B''O_6$ octahedra. According to the Glazer notation [47], the tilting system for these compounds is ($a^-a^-c^+$), indicating that the octahedra rotate along the Cartesian axes x and y in consecutive layers in opposite directions, whereas along the z-axis they rotate in the same direction. The tilting angles obtained from NPD are given in Table SI 2. As in the $La_{2-x}NiTiO_{6-\delta}$ series[23], in $La_{2-x}CoTiO_{6-\delta}$ oxides the tolerance factor slightly decreases with x as a signature of a structure becoming more and more distorted to accommodate an increasing amount of A-ion vacancies (Table SI 2). This effect is particularly evident in the octahedra tilting angles which become more different along the three Cartesian directions.

Interestingly, the change from monoclinic to orthorhombic symmetry observed upon substitution of La^{3+} by Sr^{2+} in $La_{2-x}Sr_xCoTiO_{6-\delta}$ [46] is not found in $La_{2-x}CoTiO_{6-\delta}$, this is upon A-site vacancy creation. As previously discussed, this lowering of symmetry is only related to the 3d-metals ordering. Cobalt and titanium are ordered along the entire $La_{2-x}CoTiO_{6-\delta}$ series and all these perovskites display a monoclinic symmetry with β angle close to 90°, (Table SI 1). Ordering is evidenced by the presence of the (011), (101) and (-101) peaks located at 15.4 (2θ) in the NPD pattern shown in Fig. 1 (these indices are given in the so-called diagonal perovskite cell $\sqrt{2}a_p$ x $\sqrt{2}a_p$ x $2a_p$ and correspond to $(½\ ½\ ½)_p$, $(½\ -½\ ½)_p$ and $(-½\ ½\ ½)_p$ respectively, in the cubic perovskite cell).

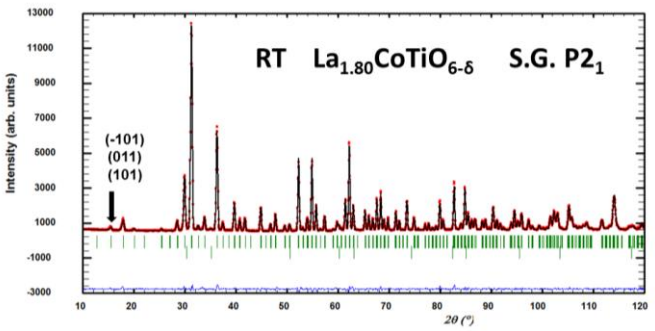

Figure 1. Room temperature experimental (red circles) and calculated (black continuous line) NPD patterns (and their difference, blue line at the bottom) for $La_{1.80}CoTiO_{6-\delta}$ using the structural model given in Table SI 1. Green vertical bars indicate the positions of the Bragg peaks for this phase; the second row corresponds to weak peaks due to Al from the experimental setup.

As the amount of La-vacancies increases, titanium and cobalt ions remain mostly ordered, and the B'-O and B''-O distances and corresponding BVSs remain clearly different. Therefore, the presence of A-site vacancies does not promote disordering of the 3d-metals in $La_{2-x}CoTiO_{6-\delta}$; interestingly, a similar behavior was observed for the analogous Ni-containing series.[23] By contrast, substitution of La^{3+} for Sr^{2+} in both parent double perovskites La_2NiTiO_6 and La_2CoTiO_6 with rock-salt like ordered B-cations substructure, induces 3d-metal disorder for a degree of substitution as low as 10%. In oxides $La_{2-x}Sr_xMTiO_{6-\delta}$ (M= Ni, Co) a random distribution of Sr and La provides the driving force to disorder the B-ions substructure.[21, 46] Thus, some kind of A-ion ordering in these defective perovskites $La_{2-x}MTiO_6$ (M= Ni, Co) will preserve the ordering of the B-ions present in the parent materials La_2MTiO_6 (M= Ni, Co). In this connection, it is well established that A-site-deficient perovskites such as $La_{0.6}Sr_{0.1}TiO_3$ [48], $RE_{1-x}MO_3$ (RE= La, Ce, Pr, Nd; M= Ti (x = 1/3), Nb (x = 2/3)) [49, 50] and $La_{2/3-x}Li_{3x}TiO_3$ [51] exhibit a layered order of A-ions and vacancies. B-cation order is quite usual in perovskites with $A_2BB'O_6$ stoichiometry [52], ordering of A ions is also frequent in $A_{1-x}\square_xBO_3$ A-site deficient perovskites and some perovskites with two kinds of A and B ions, denoted as $AA'BB'O_6$, are known to present order in both the A and B substructures [53, 54]. The common features of the three kinds of structure are rock-salt ordering of the B cations, layered ordering of the A-site cations and distortions involving octahedral tilting. Some or all of these characteristics can be present in a given compound; one example of the latter is the $La_{2-x}NiTiO_{6-\delta}$ series.[23] Thus, we fitted the XRD and NPD data for all samples using a structural model in which all these structural features coexist, together with the appropriate concentration of oxygen vacancies; the final structural parameters for this model are given in Table SI 1.

Interestingly, the introduction of low amounts of A-ion vacancies has little effect on the structure. Thus the x=0.05 member of the series and the parent material, La_2CoTiO_6, present similar concentration of Co/Ti-AS defects (ca. 7% and 9%, respectively). On the other hand, it seems that a few La-vacancies are randomly distributed and no ordering along the perovskites A-sites is observed.

By contrast, the refinement of NPD and XRD patterns of members with x≥0.10 reveals that, besides rock-salt ordering of B-site ions (Ti and Co), the A-site ions are also ordered in alternate La-rich and □-rich (□ = vacancy) layers perpendicular to the $2a_p$ cell parameter. The amount of oxygen vacancies increases with x along the whole $La_{2-x}CoTiO_{6-\delta}$ series. However, the maximum concentration of anion vacancies, given by δ = 3x/2, is not reached for any of the materials studied. This suggests that A-ion under-stoichiometry is only partially compensated by creation oxygen defects, (given by Eq. [1] in Kröger-Vink notation):

$$2\,La_{La}^{x} + 3\,O_{O}^{x} \rightarrow 2\,V_{La}^{'''} + 3\,V_{O}^{\bullet\bullet} + La_2O_3 \quad [1]$$

Thus, besides this mechanism, oxidation of Co^{2+} to Co^{3+} also seems to takes place in order to counterbalance charge deficiency due to La-vacancies, Eq. [2]:

$$2\,La_{La}^{x} + 6\,Co_{Co}^{x} + \frac{3}{2}\,O_2 \rightarrow 2\,V_{La}^{'''} + 6\,Co_{Co}^{\bullet} + La_2O_3 \quad [2]$$

Since La-vacancy defect, $V_{La}^{'''}$, is negatively charged and oxygen vacancy defect, $V_O^{\bullet\bullet}$, is positively charged, these two types of defects can be expected to be somewhat associated in these materials. Oxygen vacancies are manly produced in O(1) and O(6) sites (Table SI 1). The former would be associated to vacancies in both La(1) and La(2) positions since the oxygen atoms in O(1) sites are shared by two La(1) and two La(2). On its hand, O(6) atoms have as nearest neighbors four La(1) at the same z-level; therefore anion vacancies at these sites are located in the La(1) layers (the vacancies-rich ones). Thus, along the c-axis alternate La-rich (with some A-vacancies) and ($V_{La}^{'''}$+$V_O^{\bullet\bullet}$)-rich layers; consecutive layers of those kinds are separated by $(CoTi)O_{4-\gamma}$ layers (see Fig. 2). Anyhow, the mobility of anion-vacancies would be limited due to its association to La-vacancies.

Structure at SOFC operational temperature

To understand the electrical and electrochemical properties of a SOFC material, it is necessary to know its structure at operational temperatures as well as its thermal evolution, including thermal expansion. Since perovskite materials are prone to undergo thermally-induced phase transitions it is worth studying whether the title materials evolve when heated up to working temperatures, ca. 1073 K. Besides, oxygen loss could occur, which would have important consequences on the electrochemical properties.

Thus, SXRD and NPD experiments were performed at selected temperatures from room temperature to 1073 K on two samples: La1.95CoTiO6-δ (x=0.05) and La1.85CoTiO6-δ (x=0.15). At room temperature the former presents rock-salt ordering in B-ions and disordered A-ions, whereas in the latter both the B-ions and La and vacancies in A-sites are ordered (rock-salt and layer-like, respectively).

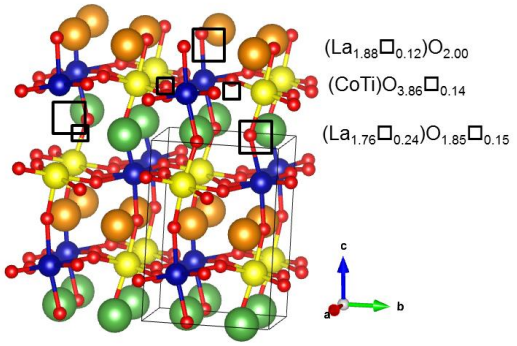

Figure 2. Schematic representation of the room temperature structure of $La_{1.80}CoTiO_{6-\delta}$.

In Figs. 3a and 3b the thermal evolution of the SXRD (222)p peak is depicted for the two samples selected. The number of reflections generated by splitting the $(222)_p$ one and the intensity ratio of these superstructure peaks (for cubic symmetry one single peak is observed), allow discriminating between the possible symmetries. At room temperature at least two peaks are clearly observed for both compositions, suggesting a pseudo-orthorhombic cell (in fact the cells are monoclinic with β≈90º). As the temperature rises the peaks tend to approach and finally one single peak is observed, this suggests a transition to a more symmetric structure, tetragonal or even cubic. It is well established in perovskites transformations responsible for phase transitions, as well as the sequences of symmetries resulting of them. In any case, the transition to a higher symmetry structure is accompanied by the disappearance of some superstructure peaks in the diffraction patterns which are mainly due to octahedra tilting and consequently to oxygen displacements.[25] To get more inside into the thermal evolution of our materials NPD thermo-diffraction experiments were performed.

Contrary to what suggested by SXRD, NPD data allow discarding any transition on heating. Indeed, Figs. 4 and SI 5 present the thermal evolution of peaks of the type $½(ooo)_p$ and $½(ooe)_p$ with h≠k (where *o* means odd, *e* even and p refers to the cubic perovskite), which are associated to anti-phase and in-phase tilting of BO_6 octahedra, respectively[25], for the x=0.05 and 0.15 member of the title series. Although for the two oxides the intensity of these superstructure maxima decreases on heating, none of them vanished, i.e. the tilting scheme remains the same from RT to 1073 K, though the magnitude of the octahedra tilting decreases. Thus, no phase transition occurs for these compounds up to SOFC-working temperatures. Even more, the $½(\pm1\ \pm1\ 1)_p$ peaks (Figs. 4b and SI 5b) also associated to rock-salt-like B-ions ordering, do not disappear suggesting that this cation-ordering remains at high temperature.

Table SI 3 presents the structural parameters obtained by the joint fitting of SXRD and NPD data for the x=0.05 and 0.15 members of the $La_{2-x}CoTiO_{6-\delta}$ series at 1073 K. Figure SI 6 shows the corresponding graphic result of the fitting of NPD data. Interestingly, the main features of the materials remain unchanged upon heating: no oxygen loss is produced; B-ions order observed at RT is preserved at high temperature and similarly A-site order observed at RT for oxides with x ≥ 0.10 seems to be preserved at least up to 1073 K.

Finally, the linear thermal expansion coefficient (TEC) was determined to range from $13.0(4).10^{-6}$ to $8.3(4).10^{-6}$ K^{-1}, for x=0.05 and x=0.20. It is worth noting that the TEC diminishes by introducing A-site vacancies, as previously reported in $(Pr_{0.6}Sr_{0.4})_{1-s}Fe_{0.8}Co_{0.2}O_{3-\delta}$ perovskites[26]. There is some controversy about the effect of A-site deficiency on the TEC since in other cases (such as $Sr(FeTi)O_{3-\delta}$) it rises as vacancies are induced in the perovskite A-sites[27]. Anyhow, from a practical point of view it is relevant that the values for the title materials are similar to that of the electrolyte CGO[28], thus avoiding the peeling off of the electrode when submitted to heating and cooling cycles under working regimes.

Cobalt oxidation state

The refined structural models on Table SI 1, obtained from NPD and XRD data, suggest that La-vacancies introduced in the parent La_2CoTiO_6 oxide induce both creation of oxygen vacancies and partial oxidation of Co^{3+}. Redox titration and thermogravimetric analyses were used to confirm the extension this latter effect occurs. Interestingly, in $La_{2-x}CoTiO_{6-\delta}$ oxides the amount of Co^{3+} is not constant with x, in contrast to what observed in the similar oxides $La_{2-x}NiTiO_{6-\delta}$ in which the amount of Ni^{3+} is low and similar for the whole series (ca. 0.7(3)% for all samples). The behavior is also different from the case of $La_{2-x}Sr_xCoTiO_{6-\delta}$ (0≤x1) in which a linear dependency of Co^{3+} content with x is found. [20] Figure 5 displays the evolution of the concentration of both Co^{3+} and oxygen vacancies along the $La_{2-x}CoTiO_{6-\delta}$ series as determined by combining TGA, NPD and titration data.

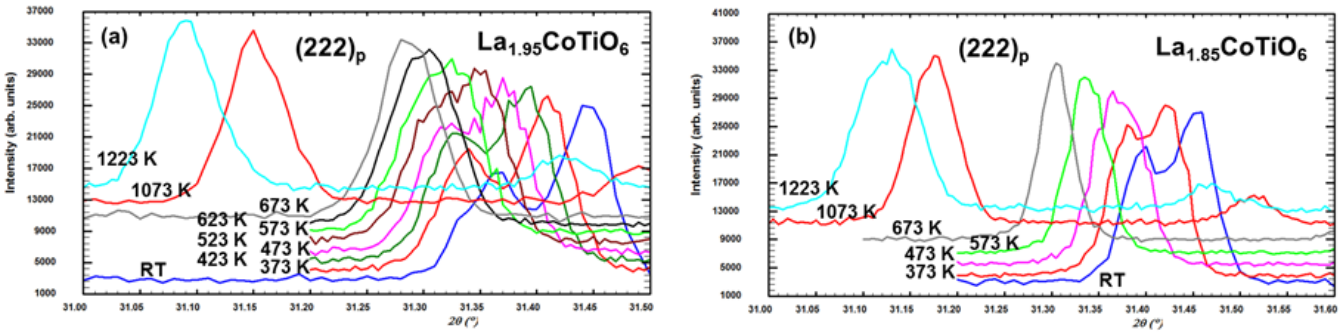

Figure 3. Thermal evolution of the $(222)_p$ SXRD peak for (a) x=0.05 and (b) x=0.15 members of the $La_{2-x}CoTiO_6$ series.

Journal Name

ARTICLE

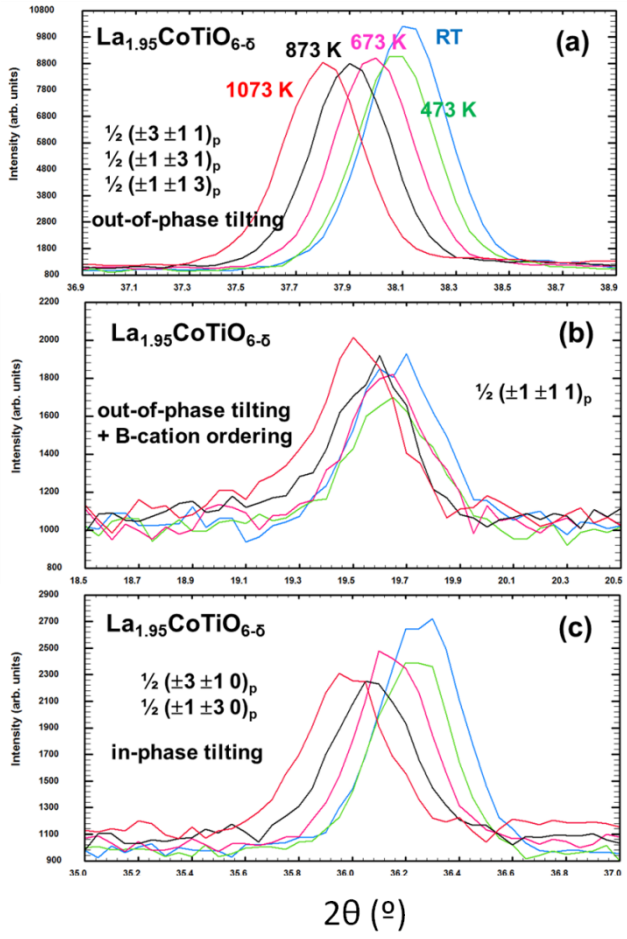

Figure 4. Thermal evolution of NPD super-structure peaks of $La_{1.95}CoTiO_{6-\delta}$ related to (a) out-of-phase octahedral tilting, (b) B-cation ordering and (c) in-phase tilting.

Figure 5 suggests that for a low level of La-vacancies (x=0.05 sample for instance) the main charge compensating mechanisms is oxidation of Co^{3+}, as given by Eq. [2]. As x increases up to a value of 0.15, the concentration of trivalent cobalt remains constant (ca. 12%) and formation of oxygen-vacancies dominates (Eq. [1]), thus δ continuously increases. For the end-member of the series, x=0.20, the amount of anion-vacancies slightly increases and the oxidation of Co^{3+} is again activated. As stated above, this behavior is different to that observed in the Ni-containing analogous, which can be explained on the basis of the different capacity of Ni^{2+} and Co^{2+} to be oxidized, easier in the latter than in the former. However, when La^{3+} is substituted by Sr^{2+} the sole operating charge-compensating mechanism along the entire $La_{2-x}Sr_xCoTiO_6$ ($0 < x \leq 1.0$) series is oxidation of Co^{3+}, with no creation of oxygen deficiency.[20]

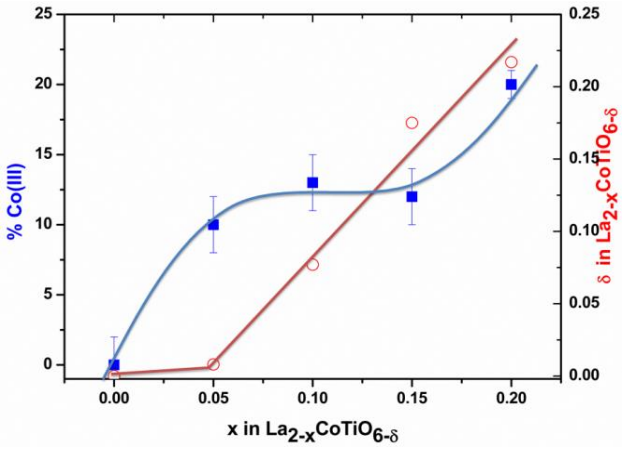

Figure 5. Evolution of Co^{3+} content and oxygen vacancies (δ) as function of A-site vacancies along the $La_{2-x}CoTiO_{6-\delta}$ series.

The presence of metals with mixed oxidation state (Co^{3+}/Co^{2+}) and oxygen-vacancies make these materials potentially interesting as MIECs electrodes[8-10].

Electrical properties

The total conductivity (σ) in air for the materials with general formula $La_{2-x}CoTiO_{6-\delta}$ (x = 0, 0.05, 0.1, 0.15, 0.2) as a function of temperature is depicted in Fig.6. The $\log_{10}$ (σT) vs. 1000/T representation shows a clear linear behavior in the temperature range under study, similar to that found for related materials: $La_{2-x}NiTiO_6$ [21, 23] and the Sr-doped series $La_{2-x}Sr_xCoTiO_{6-\delta}$.[20] This suggests that oxygen stoichiometry does not significantly change on heating, as it was also deduced from high-temperature NPD data.

Although no relevant differences of the thermal evolution of both $\log_{10}(\sigma T)$ or $\log_{10}(\sigma T^{3/2})$ are observed; on the basis of the results of similar materials[21-23] we assume the first approach, adiabatic small-polaron-hopping transport mechanism[55-57] as responsible for p-type conduction in our materials. The values of activation energies are somewhat high, ranging from 0.62-0.71 eV and similar to that reported for the parent phase, La_2CoTiO_6 [21] indicating that the same conduction mechanism is operating over the whole series.

These high activation energies may be an indication of strong trapping of electronic defects with notable reducing of the charge-carriers mobility. The introduction of vacancies in the La-position enhances the conductivity in air when compared with the parent x=0 material. Interestingly, though the conductivity of all A-deficient samples is of the same order, it seems that it increases with vacancies concentration up to x=0.1 for which a maximum in conductivity is found, as depicted in the inset of Fig. 6.

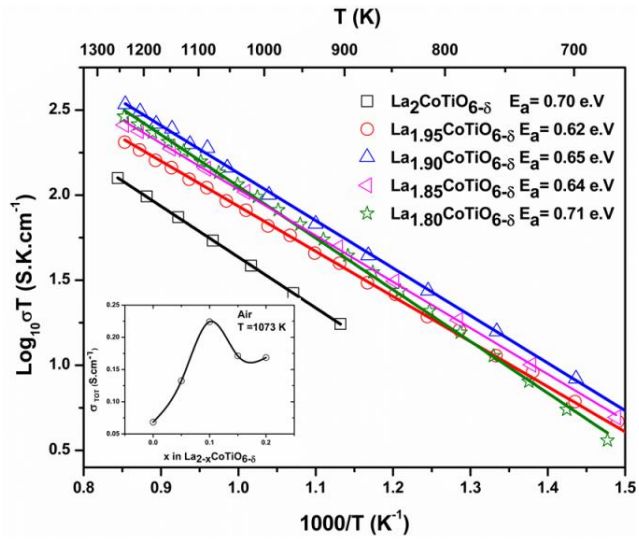

Figure 6. Arrhenius representation of the total conductivity in air for the $La_{2-x}CoTiO_{6-\delta}$ series. The inset shows the evolution of conductivity at 1073 K with A-site vacancies content.

The conductivity of some members of the $La_{2-x}CoTiO_{6-\delta}$ series at different oxygen partial pressures is presented in Fig. 7. In the high pO_2-region, the total conductivity slightly increases with pO2, indicating that transport is governed by p-type carriers (electron holes). The increase of concentration of such a type of carrier with increasing oxygen partial pressure in oxygen deficient oxides can be generally described by the defect equilibrium equation (in Kröger-Vink notation) given in Eq. [3]:

$$\frac{1}{2}O_2 + V_O^{\bullet\bullet} \rightarrow O_O^x + 2h^{\bullet} \qquad [3]$$

Alternatively, if these holes are localized the equilibrium can be expressed by the formation of Co^{3+} and concomitant filling of oxygen vacancies, as oxygen partial pressure increases from reducing conditions (Eq. [4]) :

$$2Co_{Co}^x + V_O^{\bullet\bullet} + \frac{1}{2}O_2 \rightarrow O_O^x + 2Co_{Co}^{\bullet} \qquad [4]$$

It has been demonstrated that, in the title materials, the creation of La-vacancies is compensated by two processes: the oxidation of Co^{2+} to Co^{3+} (Eq. [2]) and the creation of oxygen vacancies (Eq. [1]). Therefore, any of the two mechanisms involving oxygen-vacancies, described by Eqs. [3] and [4], may contribute to p-type electronic conduction.

The variation of p-type conductivity with pO2 follows a 1/n power law which does not correspond to the expected 1/4 or 1/6. In fact, it changes very slightly with pO2 in the measured high pO2 range. Some authors claim that this can be due to segregation of Ti or Co29, 30. In order to allow for this possibility, we checked all the samples by XRD and SEM after completion of electrical measurements and after reducing treatment for long time. Thus, Figs. SI 3 and SI 7 show the XRD pattern and SEM back-scattered, topographic electron images and EDS elemental distribution for a bar of the x=0.20 sample reduced at pO2 10-25 atm for a week. No sign of segregated phases or metal (Ti and/or Co) migration to the grain-boundaries are observed neither by XRD nor in the SEM-EDS mapping. Thus we discard these two effects. This indicates that either Co3+ is just reduced at lower pO2 or that Co3+/Co2+ oxidation/reduction process is kinetically limited under our experimental conditions. We lack data in the intermediate pO2 range, producing an apparent change of conductivity between high and low pO2 of ca. two orders of magnitude, but we know from TGA experiments that Co3+ can be effectively fully reduced at lower pO2. On the other hand, the possibility of kinetics limitation has been discarded in view of results shown in Fig. SI 8. It shows that after a change in pO2, resistance decreases exponentially. After 4 hours (the stabilization time used for the pO2 vs. conductivity measurements) it did not reach equilibrium but resistance variation is negligible. In the calculated resistance under equilibrium, variation is smaller than 8% limit and therefore log10 (σ) variation is negligible.

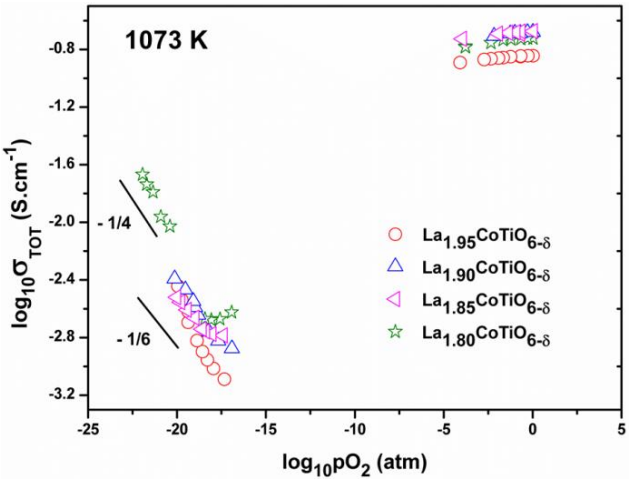

Figure 7. Conductivity as a function of the oxygen partial pressure for the $La_{2-x}CoTiO_{6-\delta}$ series

In any case, the number of p-type carrier is expected to increase as the amount of La-vacancies increases and hence total conductivity at a given pO2. This expectation is fulfilled up to x = 0.10, as shown in both Figs. 5 and 6. Several factors could be responsible for the decrease of conductivity of materials with high levels of A-vacancies. In a previous paper we reported that the Ni-related compounds present a slight Ti-overstoichiometry accompanied by segregation of small amounts of NiO. This Ti-excess partially compensates positive charge loss induced by La-vacancies creation. As a result, both,

oxidation of nickel to Ni^{3+} and creation of oxygen vacancies decrease[23]. In the present materials Ti-overstoichiometry would result in lower concentrations of p-type carriers, hence reducing the total conductivity. However, as demonstrated above, this is not the case for the title oxides, for which the actual compositions are very close to nominal. However, it is well known that point defects have strong effects not only in electrical properties but also in electrochemical properties of oxides. Thus, at low defect concentrations, conductivity increases with concentration whereas at higher concentrations, defect - defect interactions may dominate. [58, 59] This is the reason why in the search of new electrode materials for fuel cells high defect concentration is generally avoided.[44] Additionally, atomistic simulations of the related system $La_{1-x}Ni_{0.5}Ti_{0.5}O_{3-\delta}$[38, 60] suggested a strong interaction between oxygen-vacancies, lanthanum-vacancies and nickel (III) cations, yielding ternary clusters which hinder the mobility of charge carriers, and may be responsible for the low conductivity of these compounds. As a consequence, higher La-deficiency may produce a lowering in the concentration of nontrapped mobile species, thus decreasing the total conductivity and increasing the activation energy. The case for $La_{2-x}CoTiO_6$, with x>0.1 may be the same. In this connection, NPD, XRD and SEM results discard any significant segregation of secondary phases in our samples. Furthermore, crystal structure refinements revealed some association of A-site vacancies and O-vacancies (see Table SI 1 and Fig. 2) suggesting that this effect may explain the decrease of p-type conductivity for high La-vacancies concentrations.

Under stronger reducing conditions, at low oxygen partial pressure, the oxygen loss can be expressed as follows:

$$O_O^X \rightarrow \frac{1}{2}O_2 + V_O^{\bullet\bullet} + 2e' \qquad [5]$$

where the electrons are located at titanium positions as Ti^{3+} according to:

$$Ti_{Ti}^x + e' \rightarrow Ti'_{Ti} \qquad [6]$$

It is then clear from Eq. [5-6] that the total conductivity dependence under strong reducing conditions is due to n-type charge carriers (electrons). This is consistent with the low-pO_2 region observed in Fig. 7, where the conductivity increases linearly with a power-law dependence of -1/n ($6 \leq n \leq 4$) for the different compositions.

This scenario leads to formulate a defect-chemistry model that may explain the observed results.

The mass action constant of Eq. [5] can be expressed as:

$$K_O = pO_2^{\frac{1}{2}}[V_O^{\bullet\bullet}]n^2 \qquad [7]$$

where n corresponds to the concentration of electrons residing as Ti^{3+}cations.

If the compensation mechanism for La-vacancies creation is mainly governed by the oxygen vacancies incorporation in the structure [Eq. 1], then the electroneutrality will be expressed as:

$$2[V_O^{\bullet\bullet}] \approx 3[V_{La}^{'''}] + n \qquad [8]$$

The usual observance of a -1/4 power-law dependency for conductivity versus pO_2 only holds under the assumption that oxygen vacancies are constant and given by the concentration of La deficiency in as much as the number of vacancies created by the charge deficiency of La/Vac replacement is much larger than the number of Ti^{3+} that are being created upon reduction. Thus:

$$2[V_O^{\bullet\bullet}] \approx 3[V_{La}^{'''}] \qquad [9]$$

Then, the electronic carriers concentration is expressed as:

$$n \approx \frac{2K_o}{3[V_{La}^{'''}]} pO_2^{-\frac{1}{4}} \qquad [10]$$

On the other hand, if the oxygen-vacancy concentration is mainly governed by the oxygen equilibrium (Eq. [5]):

$$2[V_O^{\bullet\bullet}] \approx n \qquad [11]$$

Then, the concentration of electronic carriers can be expressed as:

$$n \approx 2K_o pO_2^{-\frac{1}{6}} \qquad [12]$$

For a general situation in which neither of these scenarios predominate the slope lies between -1/4 and -1/6.

In Fig. 7, the low-pO_2 region, presents slopes between 1/4 and -1/6 with no apparent transition to different power law in this region. Even for the composition x = 0.20, for which the data were taken even at pure H_2 atmosphere, no change in the slope tendency was observed. Then it seems that both processes: reduction of Ti^{4+} to Ti^{3+} and creation of A-site vacancies generate similar concentration of anion vacancies.

In absence of significant ionic conductivity, a change from n- to p- type semiconductivity is expected for all the samples at a relatively low-pO_2. However, in the range of measurements this is only seen at all in samples with the highest amount of La-vacancies (highest amount of oxygen vacancies). For these samples (x=0.15 and 0.2) a significant contribution of ionic conductivity can be discounted, in spite of the high amount of

oxygen vacancies. This may be due to defect clustering limiting the mobility of the oxygen vacancies.

Due to lack of data, nothing can be said for certain about the ionic conductivity of samples x=0.05 and 0.1, those with the lowest La-vacancies concentration and thus with the lowest oxygen vacancies concentration. When tested as cathodes, (see below) the lowest polarization resistance is found for x=0.05, perhaps suggesting the participation of fewer but more mobile oxygen vacancies. On the other hand, in the samples with high La-vacancies concentration, the transition from n- to p-type semiconductivity is displaced to lower pO2. This may be related to the slight increasing of p-type semiconductivity with La-vacancies concentration as it is observed in the total conductivity in air at high temperature for the $La_{2-x}CoTiO_{6-\delta}$ series (Fig. 6).

The experimental setup does not allow the establishment of stable intermediate pO_2 in order to analyze the possible contribution of ionic conductivity by observing a pO_2-independent regime. However, data obtained at low pO_2 point to a negligible contribution of ionic conductivity when compared to the n-type contribution. Therefore ionic conductivity has to be lower than 8 x 10^{-4} S cm^{-1} which is the minimum value of n-type conductivity measured for x=0.05.

The clustering of defects, mainly La- and O-vacancies, is the most likely cause of both negligible ionic conductivity and low electronic conductivity. In fact, the comparison with the system $La_{2-x}Sr_xCoTiO_6$ is relevant inasmuch as the aliovalent Sr-substitution is mainly charge-compensated by the oxidation of Co^{2+} to Co^{3+}. This produces an enhancement of the conductivity due to a higher p-type carriers concentration and displaces the n-p transition to lower pO_2 [22, 40]. By contrast, no oxygen vacancy creation is detected, avoiding the formation of this kind of clusters, substantially increasing the conductivity and also reducing the ionic contribution to total conductivity.

Chemical stability and compatibility

Prior to be used as components in SOFC cathodes the chemical compatibility of the title materials with state-of-art electrolytes (YSZ and CGO) was evaluated in simulated processing and working conditions.

Treatments in air of samples at moderate temperatures (1073 K) for several days do not produce any reaction with YSZ (XRD not shown). By contrast, firing at high temperature, ie. 1373 K, for 8 h induces reaction producing some La_2ZrO_7 (Fig. SI9). On the other hand, no reaction occurs with GCO, even when heated up at high temperature. As an example, Fig. 8 demonstrates that no additional phase is formed by firing $La_{1.90}CoTiO_{6-\delta}$ with CGO at 1373 K for 8 h.

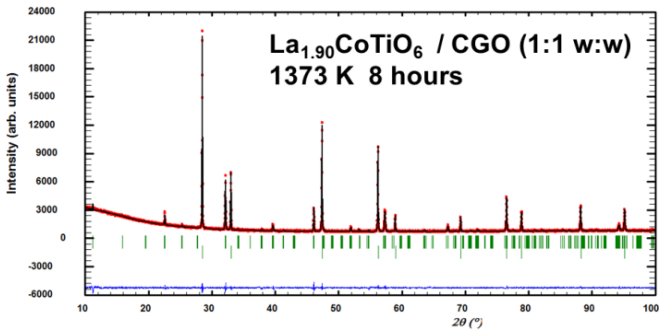

Figure 8. XRD-pattern of $La_{1.90}CoTiO_{6-\delta}$:CGO (1:1 w:w) mixture after fired at high temperature for 8 h.

Polarization tests on symmetrical cells

The temperature dependence of the polarization resistance (R_p) of symmetrical cells composed of 1:1 w/w composites ($La_{2-x}CoTiO_{6-\delta}$:CGO) over the same electrolyte (CGO) is represented in Fig. 9. A clear Arrhenius-like behavior with activation energies ranging from 1.33 to 1.62 eV is observed. The R_p values are close to or even lower than those obtained for the LSM/YSZ composite made by the same procedure (0.47 Ω cm^2 at 1073K), making these composites good candidates as cathode in a real device. The activation energies are also similar. The member with x=0.05 exhibits the lowest R_p (0.39 Ω cm^2 at 1073K) of the series, though the highest total conductivity is observed for x = 0.10 (see inset on Fig. 6). This suggests that, for x=0.05, a better balance between conductivity (both ionic and electronic) and catalytic activity is achieved. Thus, in the parent compound no mixed valence is present resulting in low conductivity. On the other hand, for x > 0.05 the observed ordering of A-site vacancies and oxygen-vacancies may result in the formation of some kind of clusters of defects[38, 60] which hinder oxide mobility and limit the catalytic activity for oxygen reduction. In this connection the close relationship between point defect and extended defect with both electrical and electrochemical properties can be recalled [44, 58, 59].

Is worth noting that commercial LSM powders, used as a reference, have optimum microstructural properties (particle size, porosity, specific surface…), whereas none of our samples present an improved microstructure (Fig. 10). In spite of this, the polarization resistance of electrodes made using the title materials are similar or even slightly better (for x=0.05) to that made of LSM.

A cross-sectional view of an electrode of composition $La_{1.90}CoTiO_{6-\delta}$:CGO (1:1 w:w) after operation is presented in Fig. 10. Good adherence between components is observed, without any noticeable defects such as cracking or delamination in the interfaces. However the microstructure is far from being optimized since large particles of the active materials are covered by submicron particles of the electrolyte. This is not a proper microstructure for obtaining optimal triple-phase boundary conditions.

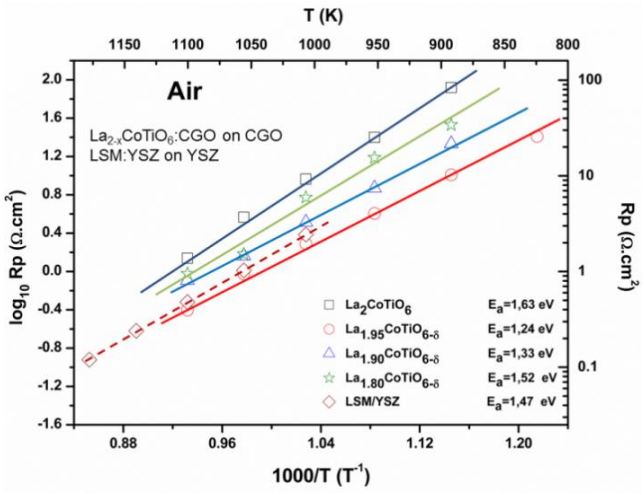

Figure 9. Temperature dependence of the polarization resistance of symmetric cells based on the $La_{2-x}CoTiO_{6-\delta}$ system on CGO electrolyte oxidant conditions. Data of LSM/YSZ cells are included for comparison

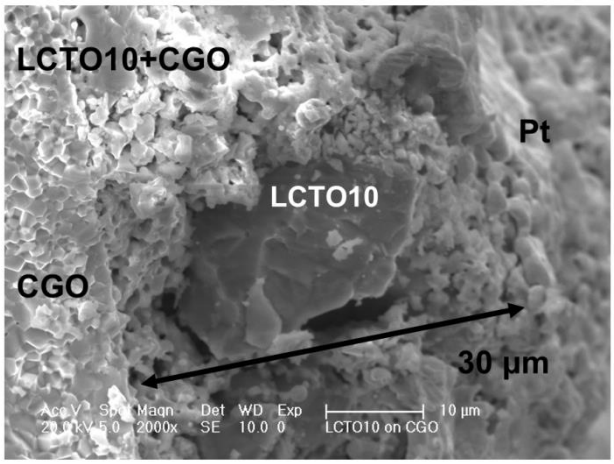

Figure 10. SEM micrograph of the (1:1 w:w) cathode $La_{1.90}CoTiO_{6-\delta}$/CGO on CGO electrolyte.

In previous papers, we reported that $La_{2-x}Sr_xNiTiO_{6-\delta}$: YSZ-based electrodes[21] exhibit polarization resistances higher than 1.5 Ω cm² under oxidizing conditions at 1073 K whereas the value for the A-site deficient compound $La_{1.80}NiTiO_{6-\delta}$ is 0.5 Ω cm² in the same conditions[23]. Thus, the creation of vacancies in the perovskite A-site seems to be a more favorable strategy for improving the electrochemical performance of perovskite systems. This is also confirmed in the present case when comparing the best polarization resistance found in the $La_{2-x}Sr_xCoTiO_6$ series (0.8 Ω cm² for x=0.4)[22] with the herein presented $La_{2-x}CoTiO_6$ series; indeed for the latter, the member with x=0.05 exhibits an even lower R_p (0.39 Ω cm² at 1073K). It is worth remarking that further improvements may be achieved through optimized morphology and electrode fabrication, making the title compounds really competitive cathode materials for SOFCs.

Conclusions

The crystal structure of the parent material La_2CoTiO_6 is kept upon La-vacancy creation with respect to cell symmetry and parameters (S.G. $P2_1/n$; $\sqrt{2}a_p$ x $\sqrt{2}a_p$ x $2a_p$) and B-cation ordering as deduced by means of XRD, SXRD and NPD. Cobalt and titanium ions are ordered, though some degree of intermixing or anti-site defects (AS) of Co and Ti on the B' and B'' sites, respectively, is present (c.a. ~9%) On the other hand, La-deficiency produces a new ordering consisting of alternating La-rich and □-rich (□ = vacancy) layers along the $2a_p$ parameter direction. Interestingly, at SOFC operational temperatures structural details are maintained and no oxygen loss has been observed.

NPD, TGA and titration analysis demonstrate that La-deficiency is compensated through two main mechanisms. The oxidation of Co^{2+} to Co^{3+} on one hand, which is predominant at low x and creation of oxygen vacancies, that predominates at intermediate x. At high x both are operating. The existence of the two extrinsic defects, Co^{3+} and oxygen vacancies, explains the variation of total electrical conductivity with oxygen partial pressure. At high pO_2 p-type semiconducting behavior arises from the existence of oxygen vacancies, and concomitant holes creation upon annihilation, and Co^{2+}/Co^{3+} equilibrium at different pO_2 conditions temperatures. An increasing of total electrical conductivity under air is observed up to x=0.1 due to increasing of both Co^{3+} and oxygen vacancies. However for x>0.1 conductivity decreases, defect clustering is likely at the origin of this behavior. In fact the ordering of alternating La-rich and □-rich (□ = vacancy) along the c-direction of the structure supports this hypothesis.

Under oxidizing conditions, $La_{2-x}CoTiO_{6-\delta}$ materials are chemically stable towards CGO whereas they react with YSZ. Using CGO as electrolyte, the best electrochemical performances, determined on symmetrical cells, are obtained for compositions with low A-site vacancy concentrations. The member with x=0.05 exhibits the lowest R_p of the series (0.39 Ω cm² at 1073K), though the highest total conductivity is observed for x = 0.10. This suggests that, for x=0.05, a better balance between conductivity (both ionic and electronic) and catalytic activity is achieved. Thus, in the parent compound no mixed valence is present resulting in low conductivity. On the other hand, for x > 0.05 the observed ordering of A-site vacancies and oxygen-vacancies may result in the formation of some kind of clusters of defects which hinder oxide mobility and limit the catalytic activity for oxygen reduction. It is worth remarking that to make the title compounds competitive cathode materials for SOFCs further improvements regarding morphology and optimization of electrode fabrication are needed.

Acknowledgements

We thank Ministerio de Economía y Competitividad and Comunidad de Madrid for funding the projects MAT2013-46452-C4-1-R, PIB2010JP-00181 and S2013/MIT-2753, respectively. Financial support from Universidad San Pablo is also acknowledged, in particular, its support to AG for a short stay at Technical University of Denmark.

Accesses to the neutron facilities at the Laboratoire Léon Brillouin and FRMII and to ESRF, is gratefully acknowledged.

References

1. Z. Shao and S. M. Haile, *Nature*, 2004, **431**, 170-173.
2. S. Tao and J. T. S. Irvine, *Nat Mater*, 2003, **2**, 320-323.
3. S. J. Skinner and J. A. Kilner, *Solid State Ionics*, 2000, **135**, 709-712.
4. A. E. York, T. Xiao and M. H. Green, *Topics in Catalysis*, 2003, **22**, 345-358.
5. S. B. Adler, *Chemical Reviews*, 2004, **104**, 4791-4844.
6. Z. Liu, M.-F. Han and W.-T. Miao, *Journal of Power Sources*, 2007, **173**, 837-841.
7. X. Sun, S. Wang, Z. Wang, J. Qian, T. Wen and F. Huang, *Journal of Power Sources*, 2009, **187**, 85-89.
8. A. Aguadero, J. A. Antonio, D. Pérez-Coll, C. de La Calle, M. T. Fernández-Díaz and J. B. Goodenough, *Chem. Mater.*, 2010, **22**, 789-798.
9. L. Yang, C. D. Zuo, S. Z. Wang, Z. Cheng and M. L. Liu, *Adv. Mater.*, 2008, **20**, 3280-3283.
10. J. M. Serra and V. B. Vert, *ChemSusChem*, 2009, **2**, 957-961.
11. K. Efimov, Q. Xu and A. Feldhoff, *Chem. Mater.*, 2010, **22**, 5866-5875.
12. L.-W. Tai, M. M. Nasrallah, H. U. Anderson, H. U. Sparlin and S. R. Sehlin, *Solid State Ionics*, 1995, **76**, 273-278.
13. J. W. Stevenson, T. R. Armstrong, R. D. Carneim, L. R. Pederson and W. J. Weber, *J. Electrochem. Soc.*, 1996, **143**, 2722-2729.
14. B. C. H. Steele, *J. Power Sources*, 1994, **49**, 1-14.
15. S. Tao and J. Irvine, *Journal of the Electrochemical Society*, 2004, **151**, A252-A259
16. H. Tu, Y. Takeda, N. Imanishi and O. Yamamoto, *Solid State Ionics*, 1997, **100**, 283-288.
17. L. W. Tai, M. M. Nasrallah, H. U. Anderson, D. M. Sparlin and S. R. Sehlin, *Solid State Ionics*, 1995, **76**, 259-271.
18. J. Canales-Vazquez, J. C. Ruiz-Morales, D. Marrero-Lopez, J. Pena-Martinez, P. Nunez and P. Gomez-Romero, *Journal of Power Sources*, 2007, **171**, 552-557.
19. J. C. P. Perez-Flores, C. Ritter, D. Perez-Coll, G. C. Mather, F. Garcia-Alvarado and U. Amador, *Journal of Materials Chemistry*, 2011, **21**, 13195-13204.
20. M. Yuste, J. C. Perez-Flores, J. R. de Paz, M. T. Azcondo, F. Garcia-Alvarado and U. Amador, *Dalton Transactions*, 2011, **40**, 7908-7915.
21. J. C. Pérez-Flores, Ritter, C., Pérez-Coll, D., Mather, G. C., Canales-Vázquez, J., Gálvez-Sánchez, M., García-Alvarado, F., Amador, U., *International Journal of Hydrogen Energy*, 2012, **37**, 7242-7251.
22. A. Gómez-Pérez, Yuste, M.,Pérez-Flores, J.C.,Ritter, C., Azcondo, M.T., Canales-Vázquez, J., Gálvez-Sánchez, M.,Boulahya, K.,García-Alvarado, F., Amador, U., *Journal of Power Sources*, 2013, **227**, 309-317.
23. J. C. Pérez-Flores, Pérez-Coll, D., García-Martín, S., Ritter, C., Mather, G.C., Canales-Vázquez, J., Gálvez-Sánchez, M., García-Alvarado, F., Amador, U., *Chemistry of Materials*, 2013, **25**, 2484-2494.
24. R. Hammami, H. Batis and C. Minot, *Surf. Sci.*, 2009, **603**, 3057–3067.
25. D. I. Woodward and I. M. Reaney, *Acta Crystallographica Section B*, 2005, **61**, 387-399.
26. K. K. Hansen, *Journal of the Electrochemical Society*, 2009, **156**, B1257-B1260.
27. V. V. Kharton, A. V. Kovalevsky, E. V. Tsipis, A. P. Viskup, E. N. Naumovich, J. R. Jurado and J. R. Frade, *Journal of Solid State Electrochemistry*, 2002, **7**, 30-36.
28. V. V. Kharton, F. M. Figueiredo, L. Navarro, E. N. Naumovich, A. V. Kovalevsky, A. A. Yaremchenko, A. P. Viskup, A. Carneiro, F. M. B. Marques and J. R. Frade, *Journal of Materials Science*, 2001, **36**, 1105-1117.
29. E. Y. Konysheva, X. Xu and J. T. S. Irvine, *Advanced Materials*, 2012, **24**, 528-532.
30. K. K. Hansen and K. V. Hansen, *Solid State Ionics*, 2007, **178**, 1379-1384.
31. N. Orlovskaya, M. Lugovy, S. Pathak, D. Steinmetz, J. Lloyd, L. Fegely, M. Radovic, E. A. Payzant, E. Lara-Curzio, L. F. Allard and J. Kuebler, *Journal of Power Sources*, 2008, **182**, 230-239.
32. K. Yamaji, T. Horita, M. Ishikawa, N. Sakai and H. Yokokawa, *Solid State Ionics*, 1999, **121**, 217-224.
33. O. Yamamoto, Y. Takeda, R. Kanno and M. Noda, *Solid State Ionics*, 1987, **22**, 241-246.
34. M. C. Brant, T. Matencio, L. Dessemond and R. Z. Domingues, *Solid State Ionics*, 2006, **177**, 915-921.
35. M. C. Brant and L. Dessemond, *Solid State Ionics*, 2000, **138**, 1-17.
36. E. Konysheva and J. T. S. Irvine, *Chemistry of Materials*, 2011, **23**, 1841-1850.
37. J. Knudsen, P. B. Friehling and N. Bonanos, *Solid State Ionics*, 2005, **176**, 1563-1569.
38. S. O. Yakovlev, V. V. Kharton, E. N. Naumovich, J. Zekonyte, V. Zaporojtchenko, A. V. Kovalevsky, A. A. Yaremchenko and J. R. Frade, *Solid State Sciences*, 2006, **8**, 1302-1311.
39. N. Q. Minh and T. Takahashi, eds., *Science and Technology of Ceramic Fuel Cells*, Elsevier, Amsterdam, Holland, 1995.
40. J. C. Perez-Flores, A. Gomez-Perez, M. Yuste, J. Canales-Vazquez, E. Climent-Pascual, C. Ritter, M. T. Azcondo, U. Amador and F. Garcia-Alvarado, *International Journal of Hydrogen Energy*, 2014, **39**, 5440-5450.
41. J. Rubio-Zuazo, Collado-Negro, V. , Heyman, C. , Ferrer,P., da Silva, I., Gallastegui, J.A., Gutiérrez-León, A., Castro, G.R. , *Journal of Physics: Conference Series*, 2013, **425**, 052005.
42. J. Rodríguez-Carvajal, *Physica B: Condensed Matter*, 1993, **192**, 55-69.
43. M. Yuste, Perez-Flores, J.C., Romero de Paz, J., Azcondo,M.T., Garcıa-Alvarado, F., Amador, U., *Dalton Trans.*, 2011, **40**, 7908-7915.

44. J. C. Ruiz-Morales, J. Canales-Vázquez, J. Peña-Martínez, D. M. López and P. Núñez, *Electrochimica Acta*, 2006, **52**, 278-284.
45. B. Raveau, Seikh, M. , *Cobalt Oxides: From Crystal Chemistry to Physics*, Wiley-VCH, Berlin, 2012.
46. A. Gómez-Pérez, J. C. Pérez-Flores, C. Ritter, K. Boulahyad, G. R. Castro, F. García-Alvarado and U. Amador, *Journal of Applied Crystallography*, 2014, **47**, 745-754.
47. A. M. Glazer, *Acta Crystallographica Section B*, 1972, **28**, 3384-3392.
48. C. J. Howard and Z. Zhang, *Journal of Physics: Condensed Matter*, 2003, **15**, 4543-4553.
49. C. J. Howard and Z. Zhang, *Acta Crystallographica Section B*, 2004, **60**, 249-251.
50. Z. Zhang, C. J. Howard, K. S. Knight and G. R. Lumpkin, *Acta Crystallographica Section B*, 2006, **62**, 60-67.
51. S. Garcia-Martin, M. A. Alario-Franco, H. Ehrenberg, J. Rodriguez-Carvajal and U. Amador, *J Am Chem Soc*, 2004, **126**, 3587-3596.
52. R. H. Mitchell, *Perovskite: Modern and Ancient*, Almay Press Inc., Ontario (Canada), 2002.
53. M. C. Knapp and P. M. Woodward, *Journal of Solid State Chemistry*, 2006, **179**, 1076-1085.
54. G. King, S. Thimmaiah, A. Dwivedi and P. M. Woodward, *Chemistry of Materials*, 2007, **19**, 6451-6458.
55. R. Koc, *J. of the European Ceramic Society,*, 1995, **15**, 867-874.
56. M. Viret, *Phys Rev B,*, 1997, **55**, 8067-8070.
57. S. Chatterjee, *Phys Rev B,*, 2000, **61**, 6106-6113.
58. A. Atkinson, S. Barnett, R. J. Gorte, J. T. S. Irvine, A. J. McEvoy, M. Mogensen, S. C. Singhal and J. Vohs, *Nature Materials*, 2004, **3**, 17-27.
59. J. Canales-Vazquez, M. J. Smith, J. T. S. Irvine and W. Z. Zhou, *Advanced Functional Materials*, 2005, **15**, 1000-1008.
60. S. Yakovlev, V. Kharton, A. Yaremchenko, A. Kovalevsky, E. Naumovich and J. Frade, *Journal of the European Ceramic Society*, 2007, **27**, 4279-4282.